ACOUSTO-OPTICAL SIGNAL PROCESSING

Acousto-optical interaction, or the interaction between sound and light, was first predicted by Brillouin in 1922 (1) and theoretically characterized by Raman and Nath in 1935 to 1936 (2–5). Almost 80 years have past since the first experimental verification of the acousto-optical effect by Debye and Sears in the United States (6) and by Lucas and Biquard in France (7). Today, acousto-optical technology has developed to the extent that it is the most mature electrical-to-optical transducer technology available. Furthermore, there has been rapid development in other optical component technologies such as lasers, detectors, integrated optics, fibers, and passive optics. This simultaneous maturing of optical technologies has led to realizing practical and powerful analog and digital signal processing systems for implementing certain computationally intensive operations that are otherwise difficult to achieve using alternative hardware technologies. For example, applications include spread spectrum communications, radar, and electronic warfare surveillance (8).

A general acousto-optical signal processing system consists of four basic components, namely, light sources, light modulation devices, passive optics, and light detection devices. The goal of the system designer is to combine the best features of the available optical components to realize a compact, robust, high speed computing system that implements the desired signal processing operation. In this article, we will highlight several acousto-optical systems for signal processing applications such as radio-frequency (RF) spectrum analysis and radar range-Doppler processing. This article describes the underlying principles and techniques that are used to construct these acousto-optical systems. First, we shall introduce the simple acousto-optical device model that is used in system analysis thoughout the article. Next, other system components are described, and important performance issues are highlighted from a designer's point of view. In addition, optical processing techniques are introduced that are used to perform the desired signal processing transformations.

THE ACOUSTO-OPTICAL DEVICE MODEL

Basic acousto-optical devices exist in three different interaction geometries defined by the value of the parameter $a = (\delta\theta_0/\theta_a)$, the ratio of divergence angles of the optical beam θ_0, and the acoustic beam θ_a. In the limit $a \ll 1$ the device acts as a optical beam deflector, while with $a \approx 1$ the device functions as a modulator. Furthermore, for the limit $a \gg 1$, the device performs as an optical filter. In this article the acousto-optical deflector (AOD), or Bragg cell, will be stressed in the optical processing systems to be described later. The name "Bragg cell" derives from the particular Bragg angle incidence operation of the acousto-optical device, where the long interaction length between the acoustic and optical waves produces a volume diffraction effect allowing only one sideband of the diffracted beam to be produced. The analysis to follow gives a simple device model for the Bragg cell. This model is adequate for initial system analysis when designing acousto-optical systems. For a more in-depth study of the acousto-optical interaction and devices, the reader is referred to articles in the optics literature (9–19).

Figure 1 shows the typical device geometry of a Bragg cell. The device consists of a transparent photoelastic crystal

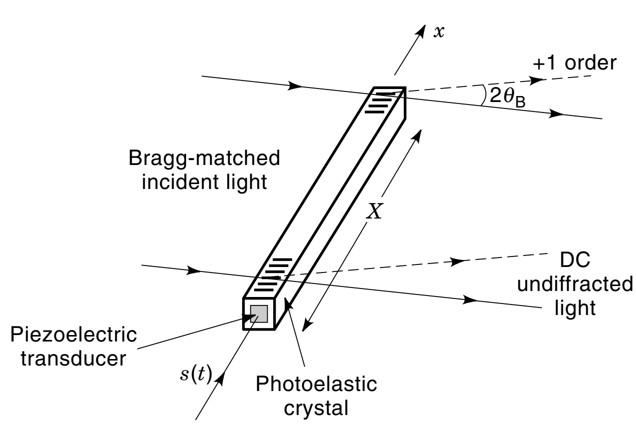

Figure 1. Device geometry of an acousto-optical Bragg cell.

whose one end is bonded to a piezoelectric transducer. A band-limited RF electronic signal $s(t)$ centered at frequency f_0 is applied to the transducer of the cell. In order to avoid nonlinear, second harmonic intermodulation terms, the bandwidth of the signal must be less than $B \le 2f_0/3$, corresponding to an octave bandwidth centered at f_0. The transducer is typically designed to have a resonant octave bandwidth centered at f_0. The RF signal applied to the transducer launches an acoustic wave replica of the signal $s(t)$ that lies within the transducer's octave bandwidth. The acoustic wave travels with a velocity v_a along the crystal length X, and it is represented along the x direction by the expression

$$u(x, t) = s\left(t - \frac{x}{v_a}\right) \mathrm{rect}\left[\frac{x - X/2}{X}\right] \tag{1}$$

where

$$\mathrm{rect}\left(\frac{x}{X}\right) = \begin{cases} 1, & \text{if } |x| \le X/2 \\ 0, & \text{otherwise} \end{cases} \tag{2}$$

An important device parameter is the acoustic delay time T_a that corresponds to the acoustic signal travel time across the finite window of the crystal. The product of the device delay T_a with the device bandwidth B gives the maximum number of resolvable analog samples that can be stored at any instant in the device. This product T_aB, also called the time bandwidth product of the Bragg cell, is an important system design parameter.

The acoustic signal induces a traveling wave volume index perturbation via the photoelastic effect in the crystal, causing a phase modulation along the crystal length that can be approximately represented as an optical transmittance function given by

$$\begin{aligned} t(x, t) &= e^{j\epsilon s(t - x/v_a)} \mathrm{rect}\left[\frac{x - X/2}{X}\right] \\ &\approx \left[1 + j\epsilon s\left(t - \frac{x}{v_a}\right) + \cdots\right] \mathrm{rect}\left[\frac{x - X/2}{X}\right] \end{aligned} \tag{3}$$

where ϵ is the modulation index that depends on the acoustic signal amplitude and the photoelastic interaction efficiency. For small diffraction efficiencies, the higher-order terms of the phase modulation expansion can be neglected, giving only the first-order traveling wave acoustic signal term $s(t - x/v_a)$. The real signal $s(t)$ can be expressed as its upper and lower sideband complex conjugate terms, because the analytic signal expansion gives $s(t) = [\tilde{s}(t) + \tilde{s}^*(t)]/2$. The transmittance of the Bragg cell can be rewritten as

$$t(x, t) = \left[1 + \frac{j\epsilon}{2}\tilde{s}(t - x/v_a) + \frac{j\epsilon}{2}\tilde{s}^*(t - x/v_a)\right] \mathrm{rect}\left[\frac{x - X/2}{X}\right] \tag{4}$$

Similarly, the signal spectrum can be written as a purely negative frequency sideband $\tilde{S}(f) = \int_{-\infty}^{0} s(t)e^{-j2\pi ft}\,dt$, and a purely positive frequency sideband can be given by $\tilde{S}^*(f) = \int_0^{\infty} s(t)e^{-j2\pi ft}\,dt$. When collimated light from a coherent source such as a laser operating at a wavelength λ and temporal frequency $v = c/\lambda$ is incident as a tilted plane wave at the negative midband Bragg angle $\theta = -|\theta_B|$, where $|\theta_B| =$

$\sin^{-1}(\lambda/2\Lambda_0) \approx \lambda/2\Lambda_0$ with respect to the acoustic propagation direction x, with the incident optical field expressed as

$$a(x, z, t) = \mathrm{Re}\left[Ae^{-j2\pi[vt - \sin\theta_B x/\lambda + \cos\theta_B z/\lambda]}\right] \tag{5}$$

the incident light is efficiently coupled into the upshifted single sideband of the first-order diffracted wave. In other words, when the optical field is incident at the negative Bragg angle on the thick index perturbation, with the x component of optical field counterpropagating with respect to the acoustic wave direction, the last term in Eq. (4) produces negligible diffraction, and the optical field is said to undergo +1-order diffraction represented by the purely negative sideband of the signal. This purely negative frequency sideband is responsible for a Doppler upshifting of the optical carrier, because the analytic representation of the optical carrier is chosen as a negative temporal frequency. When the incident optical field is incident at the positive Bragg angle, the first signal term in Eq. (4) gives negligible diffraction, and the diffracted optical field from the last term in Eq. (4) is downshifted. Thus, the light modulated by the Bragg cell can be approximately expressed as the product of the incident optical field with the appropriate single sideband transmittance of the Bragg cell. For a +1-order upshifted Bragg geometry, the emerging optical field is given by

$$\begin{aligned} b(x, z, t) &= a(x, z, t)t_+(x, t) \\ &\approx Ae^{-j2\pi[vt - \sin\theta_B x/\lambda + \cos\theta_B z/\lambda]}\left[1 + \frac{j\epsilon}{2}\tilde{s}(t - x/v_a)\right] \\ &\quad \mathrm{rect}\left[\frac{x - X/2}{X}\right] \end{aligned} \tag{6}$$

where the explicit notation of the real part of the coherent optical field has been dropped for analysis purposes in this article. The expression in Eq. (6) consists of (1) an undiffracted term that propagates along the input angle $-\theta_B$ and (2) a Doppler upshifted first-order diffracted term centered around the midband angle $+\theta_B$. Here the midband acoustic wavelength Λ_0 equals v_a/f_0, where f_0 is the midband frequency of the Bragg cell. To see the effect of Doppler upshifting, as well as beam deflection, let's consider a single-tone input signal at the frequency f. For $s(t) = \cos(2\pi ft) = [e^{j2\pi ft} + e^{-j2\pi ft}]/2$, the diffracted field is given by

$$\begin{aligned} d_f(x, z, t) &= Ae^{-j2\pi[vt - \sin\theta_B x/\lambda + \cos\theta_B z/\lambda]}\,\frac{j\epsilon}{2}\,e^{-j2\pi f(t - x/v_a)} \\ &\quad \mathrm{rect}\left[\frac{x - X/2}{X}\right] \\ &= A\,\frac{j\epsilon}{2}\,e^{-j2\pi[(v+f)t + (f - f_0/2)x/v_a + \cos\theta_B z/\lambda]} \\ &\quad \mathrm{rect}\left[\frac{x - X/2}{X}\right] \end{aligned} \tag{7}$$

where the device has been Bragg-matched for the midband frequency f_0 with the $+\theta_B = \sin^{-1}(\lambda f_0/2v_a) \approx (\lambda f_0/2v_a)$. Note that the temporal frequency of the field has increased by an amount equal to the input temporal frequency, resulting in a positive Doppler shift. Also, the angular spatial frequency of diffraction is linearly related to the input signal frequency. Thus, the diffracted optical field emerging from the Bragg cell has been temporally and spatially modulated by the input signal $s(t)$. Dropping the z propagation term for simplicity, the diffracted optical field for an input signal $s(t)$ at midband frequency f_0 can be expressed as

$$d(x, t) = A\frac{j\epsilon}{2}\,e^{-j2\pi[vt - f_0 x/2v_a]}\tilde{s}(t - x/v_a)\mathrm{rect}\left[\frac{x - X/2}{X}\right] \tag{8}$$

This is the basic modulation introduced by a Bragg cell, where the diffracted optical field is a windowed traveling-wave replica of the single sideband of the octave bandwidth input signal $s(t)$. This diffracted field experiences a temporal frequency shift equal to the signal frequency and is spatially deflected by an angle proportional to the signal frequency. These two properties of the Bragg cell form the basic optical modulation techniques that are used to accomplish various signal processing tasks throughout this article. A simpler model of the Bragg cell drops the optical carrier term, along with the multiplicative constants, and the optical axis is aligned with the input signal direction. This gives the diffracted field from the Bragg cell:

$$d(x, t) = \tilde{s}(t - x/v_a)\mathrm{rect}\left[\frac{x - X/2}{X}\right] \tag{9}$$

In general, this expression will be used in the analysis of acousto-optical systems to be described in this article. Sometimes, it is convenient to reference the window function at the center of the AOD. In this case, the diffracted field is expressed as

$$d(x, t) = \tilde{s}(t - x/v_a - T_a/2)\mathrm{rect}\left[\frac{x}{X}\right] \tag{10}$$

where $T_a/2$ is the acoustic time delay from the transducer end of the device to the center of the cell.

From coupled mode theory of the Bragg interaction in the thick isotropic acousto-optical medium (17), we can express the diffracted field amplitude $A_d(\nu)$ normalized by the incident field amplitude A_i as

$$\frac{A_d(\nu)}{A_i} = -j\,\frac{c\nu}{|c\nu|}\sin(|c\nu|L) \tag{11}$$

where ν is the applied acoustic signal voltage, L is the interaction length in the crystal, or the transducer width, and c is the coupling constant per unit applied voltage, which depends on parameters such as crystal photoelastic constant and piezoelectric coupling efficiency (9,19). Figure 2(a) shows the behavior of the normalized diffracted field amplitude with applied acoustic voltage as expressed in Eq. (11). Note that for small diffraction efficiencies (≤10%), the optical field amplitude varies linearly with the applied acoustic signal amplitude. This property of the device permits its use in implementing linear electrical to optical signal transformations. The diffraction efficiency based on the ratio of the diffracted light intensity to the incident light intensity is given by

$$\frac{I_d(\nu)}{I_i} = \sin^2(|c\nu|L) \approx (|c\nu|L)^2 \tag{12}$$

and is plotted against applied acoustic power in Fig. 2(b). Here, the diffracted light intensity varies linearly with acous-

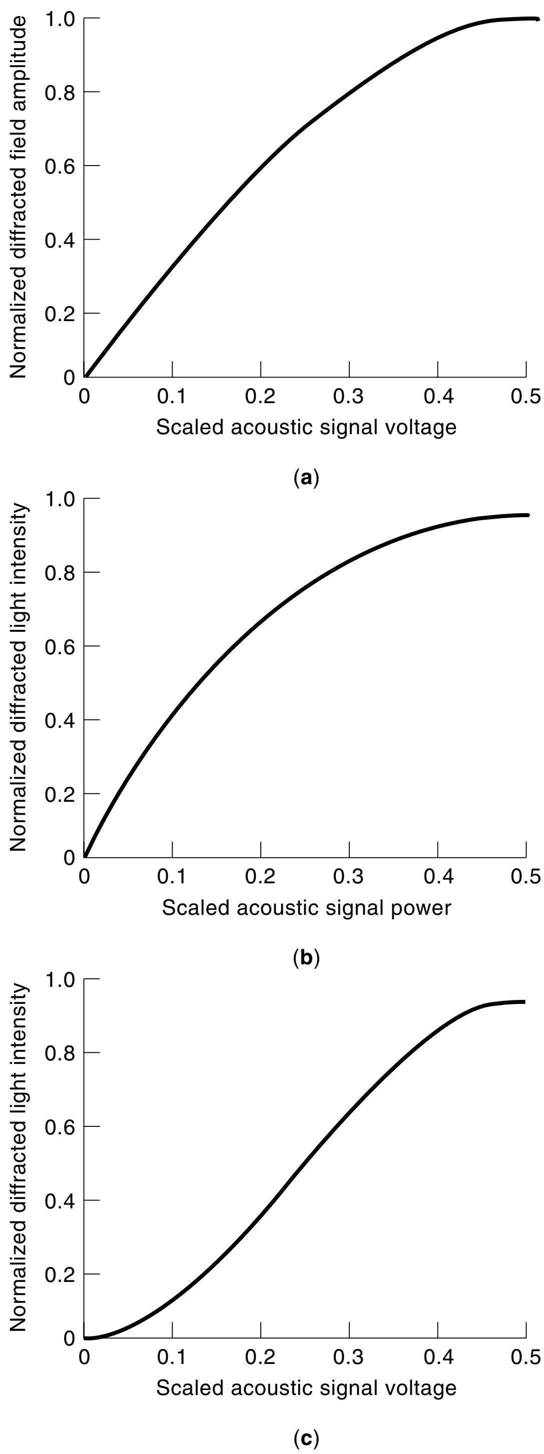

Figure 2. Plots show different acousto-optical device response curves: (a) Behavior of the normalized diffracted field amplitude with applied voltage. (b) Behavior of the normalized diffracted light intensity with applied acoustic power. (c) Behavior of the normalized diffracted light intensity with applied acoustic voltage.

tic power for small diffraction efficiencies corresponding to small arguments of the sine function. Another approach to obtaining linear intensity modulation is shown by the curve in Fig. 2(c), where the desired modulating signal amplitude is biased around the linear region of this diffracted intensity versus acoustic amplitude curve (19,20). Certain drawbacks of this bias-dependent intensity modulation scheme include small modulation depth, large bias signal requirements, and large acoustic power-related problems such as nonlinear acoustic effects in the crystals.

Commercially available Bragg cells come in a variety of specifications. Typical materials used for the crystals include fused silica, tellurium dioxide, gallium phosphide, and lithium niobate. Devices exist in large-aperture, high-resolution, high-diffraction-efficiency designs, as well as in wide-bandwidth designs (21–23). For example, devices exist with bandwidths ranging from 30 MHz at f_0 = 50 MHz to 2 GHz at f_0 = 3 GHz. Typical device storage capability or space bandwidth product is around 2000 for large-aperture cells. Apart from single-channel cells, certain companies are providing multichannel Bragg cells. For instance, a 32-channel, f_0 = 400 MHz multichannel device is available (22). Recently, a two-dimensional (2-D), single element, acousto-optical beam deflector has been introduced (21,24). Unlike one-dimensional (1-D) AOD, this 2-D AOD is capable of deflecting laser beams in 2-D space. The acousto-optical devices described to this point have been bulk devices, as an unguided acoustic wave travels though a thick crystal. Another sister technology not discussed in this article, called the surface acoustic wave (SAW) device technology, exists along side the bulk technology. The basic principles of the SAW technology are similar to the bulk technology and are described in detail in the literature (25,26). In SAW devices, the acousto-optical interaction is in a 2-D planar geometry, and not in a three-dimensional (3-D) volume. This results in miniaturization of the acousto-optical device. Today, many robust, vibration-resistant integrated optical SAW-based signal processors have been reported (27–29).

ACOUSTO-OPTICAL SYSTEM COMPONENTS AND ISSUES

Typical sources used in acousto-optical processing systems include semiconductor laser diodes, gas lasers, and semiconductor light-emitting diodes (LEDs). Small physical size (300 μm $\times$ 10 μm $\times$ 50 μm), direct pumping by low-power electric currents (15 mA at 2 V), high electrical-to-optical conversion efficiency ($\geq$20%), direct light modulation capability exceeding 10 GHz rates, and monolithic integration with other III–V semiconductor optical and electronic devices to form optoelectronic circuits make semiconductor laser diodes the most attractive light source for practical acousto-optical processing systems (30). Compared to LEDs that have a large light-emitting area ($\approx$1 mm^2) and a broad spectral width ($\approx$50 nm), laser diodes typically have 1 nm to 5 nm spectral widths, with a higher light directivity, allowing for applications in coherent optical processing, where temporal and spatial coherence of the light source plays an important role in system performance (30–34). Nevertheless, LEDs are very inexpensive, highly reliable, visible/infrared, incoherent light sources that are used in incoherent, intensity-based optical processing (35).

The laser diode can also be used in a pulsed mode, where an appropriately biased narrow pulse signal drives the diode junction. This approach is used in some acousto-optical spectrum analysis processors, where the pulsing action of the laser diode is used to freeze the traveling acoustic signal in the

AOD while simultaneously freezing heterodyne signal frequency components to baseband (36,37). Unfortunately, the pulsing action adversely affects the temporal coherence of the laser diode. This problem is mainly due to interpulse modal hopping and frequency drifting and can be reduced by biasing the laser just below threshold, with the drive signal rise time and pulse amplitude carefully adjusted (38). Optical detection in acousto-optical systems is typically achieved by semiconductor high-speed point detectors and 1-D/2-D charge coupled devices (CCDs) (30,31). The present CCD technology is mature, with devices like the Tektronix CCD, which has 2048 $\times$ 2048 pixels (39). Important system issues associated with optical detection devices include optical signal-to-noise ratio of the detected image, noise from driving electronics, spectral responsivity, rise time/bandwidth, pixel size, and photo response linearity (40–42).

Apart from using acousto-optical devices as spatial and temporal light modulators in optical processing systems, other device technologies such as liquid crystals, magneto-optics, photorefractives, and micromirrors are also being incorporated into various acousto-optical processing architectures (43). For instance, the application of optical disk and photorefractive technologies has been investigated for acousto-optical spectrum analysis (44,45). In this case, the high storage density and angular motion of the optical disk is used for reference signal generation in optical spectrum analysis. Also, the application of photorefractive crystals as time-integrating bias removers in interferometric acousto-optical correlators has been studied (46).

OPTICAL PROCESSING TECHNIQUES

Optical processing techniques can be divided into three main categories. Space processing shown in Fig. 3(a) involves the mapping of light from one spatial region A at $z = z_0$ along the optic axis z, to another spatial region B at $z = z_0'$. Typical mappings include spatial Fourier transforming, imaging, and free space Fresnel transformations. The classic space processing element is the space integrating spherical lens (47). When used in the appropriate configuration, the spherical thin lens can be used as a powerful 2-D spatial Fourier transformer, as shown in Fig. 3(b), or as an imaging/interconnection device, as displayed in Fig. 3(c). The architecture in Fig. 3(b) forms the basic building block of 2-D space-integrating spectrum analysis (47). When an input with amplitude transmittance $f(x, y)$ is placed at the front focal plane of a spherical lens of focal length F, the back focal plane produces the coherent 2-D spatial Fourier transform of $f(x, y)$. In other words, the lens implements the linear transformation:

$$F(u, v) = \int_{-\infty}^{+\infty} \int_{-\infty}^{+\infty} f(x, y) e^{-j(2\pi/\lambda F)(xx' + yy')}\, dx\, dy \qquad (13)$$

where λ is the wavelength of the coherent light, x and y are the spatial coordinates of the input plane, and $u = x'/\lambda F$ and $v = y'/\lambda F$ are the output plane spatial frequency coordinates. The ability of a lens to map spatial frequency components at the input Fourier plane to spatially separated frequency components at the output Fourier plane makes possible certain spatial operations. For example, input spatial data can be spatially separated into parallel output plane channels by using spatial frequency multiplexing of the input Fourier plane data (48). In addition, Fourier plane spatial filtering can be accomplished to alter or remove certain input signal spatial features (49). Figure 3(c) shows the imaging operation, another powerful linear 2-D spatial transformation by a spherical lens (33). Here, with the imaging condition, $1/d_i + 1/d_0 = 1/F$, satisfied, the output plane contains an inverted, scaled, diffraction limited replica of the input image. This operation is readily used to Schlieren image the acoustic traveling waves in a Bragg cell to other processing planes. In addition, the imaging operation is also used for interconnecting points in the input image plane to certain points in the output image plane. The lens has been used extensively in numerous acousto-optical space processing architectures for signal and image processing (27,50–58), and it has recently been used in neural network processors (59–62).

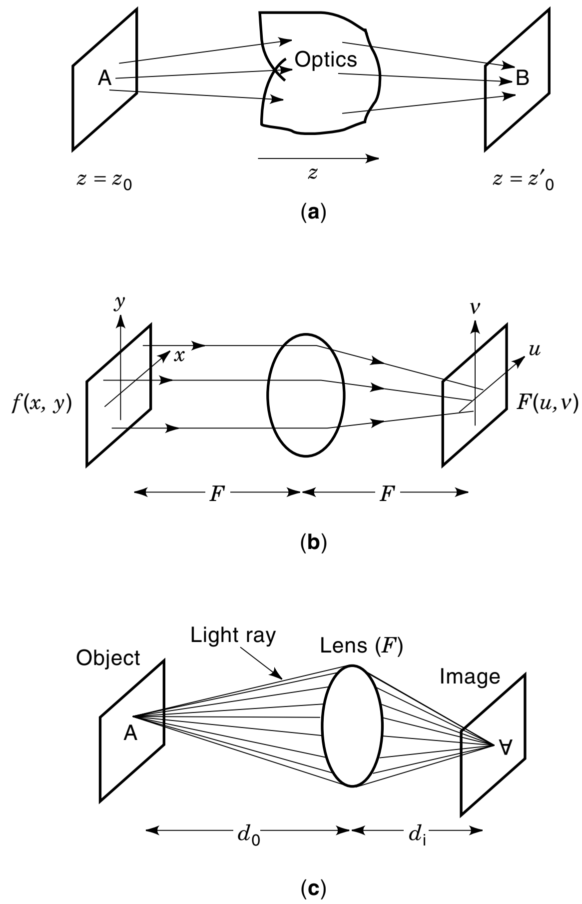

Figure 3. (a) Optical space processing. (b) Spherical lens as a two-dimensional spatial Fourier transformer. (c) Lens as an imaging/interconnection device.

From the linearity of the free space wave equation, light propagation in a coherent optical system can be modeled as a linear system represented by the superposition integral:

$$E(x', y') = \int_{-\infty}^{+\infty} \int_{-\infty}^{+\infty} h(x', y'; x, y) E(x, y)\, dx\, dy \qquad (14)$$

where $E(x, y)$ is the input plane optical field, $h(x', y'; x, y)$ is the free space impulse response for optical propagation, and $E(x', y')$ is the output plane optical field after light propagates a distance z in the optical system. For the special Fresnel diffraction case, we have

$$h(x',\, y';\, x,\, y) = \frac{e^{jkz}}{j\lambda z} \exp\left[j\frac{k}{2z}[(x'-x)^2 + (y'-y)^2] \right] \qquad (15)$$

where $h(x', y'; x, y) = h(x' - x, y' - y)$ is a linear, shift-invariant impulse response, and the wave number k equals $2\pi/\lambda$. This linear shift-invariant property of the Fresnel propagation allows the optical system designer to use Fourier domain frequency analysis techniques associated with linear time-invariant systems theory (33). In this article, a variety of different space processing techniques will be used to accomplish the desired linear transformations.

Apart from the 2-D coordinate space that is available to an acousto-optical system designer, time provides another important degree of freedom to the system architect. Time can be used to optically process information in discretized steps or continuously. Over the years, a variety of temporal processing schemes have been devised (63). Here, we will briefly highlight some of these time-processing techniques. For instance, repetitive pulsing of a light source can be used to divide a long time signal into smaller duration signals, which can be represented in the finite window of an acousto-optical system. Thus, this repetitive pulsing technique converts an otherwise large time bandwidth product signal into a smaller space bandwidth product signal that exists as a space–time rastered signal in the optical system. Pulsing can also be used to heterodyne temporal signal spectrums to baseband via the Nyquist limited aliasing phenomenon. In addition, pulsing is used to freeze acoustic signals in Bragg cells for Schlieren imaging. This repetitive signal freezing and imaging results in a temporally modulated spatial light distribution. This technique is used to implement the discrete Fourier transform (DFT) algorithm using spatial optics and time (44,64,65). Because Bragg cells represent continuously traveling acoustic waves in time, continuous time processing plays an important role in a certain class of processors. For example, in time-integrating acousto-optical correlators, the continuous nature of the operation allows for an almost unlimited correlation time window, finally limited by the dynamic range of the time-integrating detector (66).

Optical detectors play an important role in time processing, and they can be utilized in a variety of modes. An optical detector can be used to continuously collect spatially processed light for further temporal integration over a desired coherent frame time. For instance, a time-integrating 2-D CCD array can be used to implement the DFT algorithm to complete the 2-D space–time Fourier transform operation (67). The CCD can also be used in a special time-delay and integrate (TDI) or scrolling mode where integrated charge is sequentially shifted and added to previously accumulated charge along a CCD dimension (68). This type of TDI CCD photodetector has been used to implement incoherent correlation operations (69). Another light-detecting element is the high-speed photodetector that produces an electric current that is modulated by the intensity-modulated signal incident on the detector photosensitive surface. This type of high-speed optical detection is used in acousto-optical phased array radar processors (70). Also, the current generated from these high-speed point detectors can be collected in an external charging circuit to implement longer signal-processing frame times. This approach has been used in continuous-wave optical-disk-based spectrum analyzers (44). Unfortunately, optical detectors react to light intensity, which is a positive quantity. This makes it necessary to represent bipolar signals with a bias term, making the DC bias an unwanted, yet necessary, term in time-integrating processors. In the past, two electronic techniques have been employed for bias removal. They involve either (a) two CCDs or computer-based bias substraction (71) or (b) electronic carrier demodulation and filtering. Photorefractive crystals can also be used for bias removal in interferometric acousto-optical systems (72).

The unavailability of high-quality, fast, 2-D spatial light modulators, along with the presence of the highly mature, 1-D, real-time, acousto-optical spatial light modulator technology, has led to the concept of 2-D optical processing using 1-D devices (73). The spatial dimension of the acousto-optical device, coupled with time as the other orthogonal dimension, is used to transduce very large time bandwidth product signals such as images and long 1-D signals into the optical processing system. This real-time, simultaneous, time- and space-processing technique allows for multidimensional optical processing. In particular, time- and space-integrating (TSI) optical architectures have been combined to provide wideband, high-resolution, 2-D optical spectrum analysis of large time bandwidth product signals (74–78). The hybrid time- and space-processing approach combines some of the best features of both space processing and time processing, respectively. For example, space processing provides an extremely high instantaneous data throughput, while time processing allows for very large processing windows. These attributes of time and space processing allow for wide-bandwidth, high-resolution, optical spectrum analysis.

RADIO-FREQUENCY SPECTRUM ANALYSIS USING ACOUSTO-OPTICAL DEVICES

Although incoherent light has been used in acousto-optical signal processing (35), most acousto-optical systems have been built with coherent sources such as laser diodes and gas lasers. Hence, we will highlight coherent light-based acousto-optical systems.

So far, most work using acousto-optical devices has been conducted for the wide instantaneous bandwidth RF spectrum analysis operations (79,80). The most common acousto-optical spectrum analyzer is the Bragg mode acousto-optical power spectrum analyzer shown in Fig. 4(a) that is a space-integrating architecture. Here, the RF signal to be analyzed feeds an AOD that is oriented so it is Bragg-matched to the incident collimated light of wavelength λ from a coherent source such as a laser. This acousto-optical spectrum analyzer design takes advantage of the acousto-optical drive-frequency-dependent beam deflection property of the Bragg cell and the space-integrating property of a lens. Essentially, the Bragg diffracted beam undergoes an angular deflection relative to the incident collimated beam where the deflection angle is linearly proportional to the acousto-optical drive frequency f. By placing a lens one focal length F in front of the Bragg cell, the Fourier plane of the lens a distance $2F$ from the acousto-optical device contains the spatially distributed temporal spectral components of the input RF signal. Typically, a light intensity detector spatially resolves these fre-

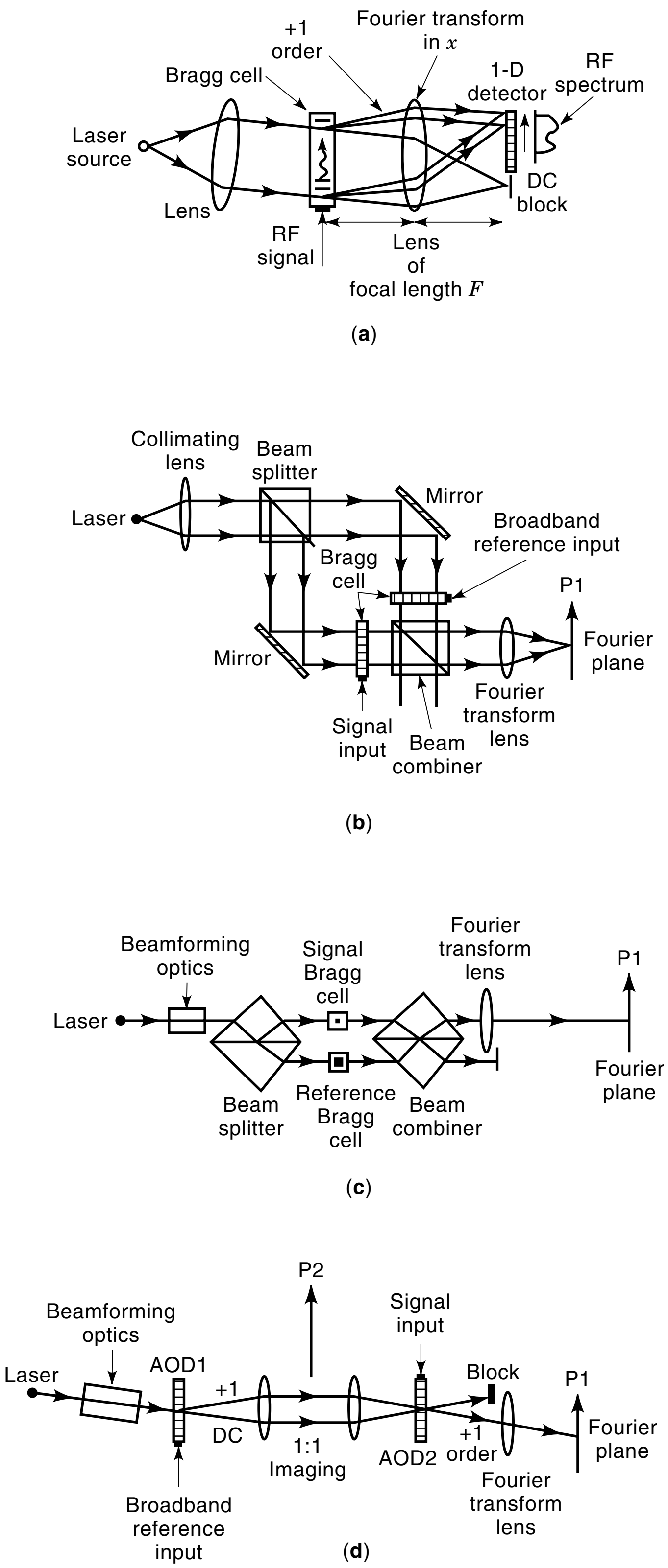

Figure 4. (a) The Bragg-mode acousto-optical power spectrum analyzer. (b) The basic Vander Lugt Mach–Zehnder interferometric spectrum analyzer. (c) The compact in-line additive Koontz interferometric spectrum analyzer. (d) The high-optical-efficiency in-line additive Riza interferometric spectrum analyzer.

quency components and provide a snapshot of the instantaneous power spectrum of the input RF signal. At the detector plane, the distance between the focused undiffracted beam spot and the diffracted spectral spot is approximated, given by $(F\lambda f)/v$.

The acousto-optical power spectrum analyzer (PSA) suffered from limited dynamic range (25 dB to 35 dB) because of (1) the squaring operation on the instantaneous spectrum of the input signal and (2) the inherent limited dynamic range of the photodetectors. Later, an interferometric technique was introduced that greatly increased the system dynamic range because the interferometric output signal was proportional to the instantaneous magnitude of the signal spectrum (81). Nevertheless, this system had a limitation because the interference output signal is generated on a rather high frequency that varies as a function of the input signal frequency. This put a high bandwidth requirement on the photodetectors. In 1981, Vander Lugt introduced an interferometric spectrum analyzer (ISA) [see Fig. 4(b)] that uses a spatially and temporally modulated reference beam to generate a much-lower-frequency interferometric signal that remains fixed in frequency over the entire signal spectrum (82). This system has received considerable attention, and many working models have been built with increased dynamic range (e.g., 58 dB) (83–85). Nevertheless, this Mach–Zehnder design (82) ISA had optical efficiency and mechanical stability limitations. Another ISA design is the compact, in-line architecture implemented by M. D. Koontz and shown in Fig. 4(c) (86). In principle, this system is similar to the Mach–Zehnder design, except the input laser beam is split into two beams that travel along the same direction, separated by a fixed distance. Here, the two Bragg cells are placed in a common plane along the optical path, and the diffracted light signals are combined and made collinear by a beam combiner. If we assume the same optical parameters as for the Mach–Zehnder system components, the Koontz in-line ISA has the same overall system optical efficiency, although with improved compactness and mechanical stability. Note that for both these ISA systems, depending on the beam combining ratio, almost half the available processed light power can be lost at the output beam combiner. Later, N. A. Riza introduced an in-line high optical efficiency ISA (87) shown in Fig. 4(d). The key feature of this architecture was its efficient use of the diffracted and undiffracted light signals from the Bragg cells, along with the removal of beam splitters and beam combiners that were required in earlier designs. Here, the AODs perform the beam splitting and beam combining. This results in a system with higher overall optical efficiency, leading to a more optimum use of the limited laser power. Other works in acousto-optical spectrum analysis are described in Refs. 88–97.

ACOUSTO-OPTICAL CORRELATORS

Correlation is a fundamental operation in signal processing, with applications in radar, communications, and pattern recognition. Over the years, various optical architectures for 1-D correlation using acousto-optical devices have been proposed and demonstrated (72,98–107). In addition, 1-D acousto-optical correlators have also be used to perform 1-D signal spectrum analysis using the Chirp-Z algorithm (108). Reference 109 gives an excellent, up-to-date account of the developments in the field of acousto-optical signal processing, particularly acousto-optical space- and time-integrating correlators. The motivation for developing acousto-optical-device-based correlation systems was in the real-time, wide instantaneous bandwidth nature of acousto-optical devices that could give large (e.g., 10^6) time-bandwidth product real-time correlations of wide instantaneous bandwidth (e.g., 500 MHz) signals.

Before we begin, its useful to describe the correlation operation, and how the Chirp-Z algorithm is used for signal spectrum analysis. For real signals $s_1(t)$ and $s_2(t)$ and, the cross-correlation function $S_{12}(\tau)$ has the form

$$S_{12}(\tau) = \int_{-\infty}^{+\infty} s_1(t-\tau)s_2(t)\,dt \tag{16}$$

which in terms of the analytic signals $\tilde{s}_1(t)$ and $\tilde{s}_2(t)$ can be written as the real value of the complex correlation function, that is,

$$S_{12}(\tau) = \frac{1}{2}\mathrm{Re}\left\{\int_{-\infty}^{+\infty} \tilde{s}_1^*(t-\tau)\tilde{s}_2(t)\,dt\right\} \tag{17}$$

where $s_1(t) = \mathrm{Re}\{\tilde{s}_1(t)\}$ and $s_2(t) = \mathrm{Re}\{\tilde{s}_2(t)\}$, and Re stands for real value. When a time-integrated correlation is implemented using AODs, the variable τ is a function of the AOD spatial coordinate x and the acoustic velocity v_a; for instance, $\tau = (2x/v_a)$, with x also being the output detector spatial coordinate (perhaps with optical magnification or demagnification). In a radar ranging application, for instance, the position of a correlation peak on the detector array corresponds to a particular range delay of the target echo signal.

The time-integrated correlator can also be used to implement time-integrating signal spectrum analysis via the Chirp-Z algorithm, which is based on a reformation of the Fourier transform integral $S(f)$ given by

$$S(f) = \int_{-\infty}^{+\infty} s(t)\exp(-j2\pi ft)\,dt \tag{18}$$

If we write $2ft = f^2 + t^2 - (t-f)^2$, $S(f)$ can be rewritten as

$$S(f) = \exp(-j\pi f^2)\int_{-\infty}^{+\infty} s(t)\exp(-j\pi t^2)\exp(j\pi(t-f)^2)\,dt \tag{19}$$

Thus, to get the Fourier transform of the input signal $s(t)$, first we premultiply the input signal with a chirp signal $\exp(-j\pi t^2)$ [or a linear frequency modulation (FM)], then correlate the product with a second chirp $\exp(-j\pi t^2)$, and finally postmultiply the result with a third chirp $\exp(-j\pi f^2)$. This sequence of operation (which includes the important correlation operation used for chirps) gives us the Fourier transform of the input signal $s(t)$. Using, for instance, a two acousto-optical-device-based correlator design, it is possible to implement the Chirp-Z transform by (1) intensity-modulating the processor light source with the signal to be Fourier-transformed and (2) feeding the same chirp signals to the acousto-optical devices to form counterpropagating chirps in space, thereby implementing the required correlation of chirps. The main advantage of the time-integrating acousto-optical spectrum analyzer is its appreciably better (e.g., 100-fold improvement) signal analysis frequency resolution when compared to an acousto-optical space-integrating spectrum analyzer that uses a Fourier transform lens for separating the Fourier components of the input signal. Such systems have been built using both bulk acousto-optical devices and integrated SAW devices and are well-characterized in the literature. We highlight three time-integrating acousto-optical correlator designs that have been the subject of considerable investigation.

One correlator design is by Montgomery (101) [see Fig. 5(a)] that uses two back-to-back, counterpropagating signal orientation, Raman–Nath mode operation acousto-optical devices placed in an intensity imaging architecture using a spatial filter in plane P to remove undesired bias and cross-product terms. The time-integrated cross-product intensity terms at the output plane of the processor produce the desired correlation result between the input signal and reference.

Another time-integrating correlator design [see Fig. 5(b)] proposed by Sprague and Koliopoulos (102) uses only one acousto-optical device operated in the Bragg mode, with the device producing a linear intensity modulation for the input signal such as a radar return. The reference signal is used to intensity-modulate a point modulator such as a laser diode. Again, imaging of the acousto-optical device onto the time-integrating detector array is used to produce the correlation operation.

More recently, N. A. Riza proposed a variant of the two acousto-optical-device time-integrating architecture where the use of the two acousto-optical devices in an interferometric design allows for linear phase and amplitude modulation of the signal and reference waveforms, without requiring bias level signals (110). Previous correlator designs required the bias levels in the modulating signals because they used intensity modulation of light source and/or acousto-optical devices. This newer correlator architecture shown in Fig. 5(c) optimizes the required minimum bias level in the output correlation signal, thus increasing the useful dynamic range of the processor. Various applications of this in-line architecture have been reported in the literature (111–118).

Two-Dimensional Signal Processing Using One-Dimensional Acousto-optical Devices

Since the mid-1970s, various acousto-optical processors have been proposed for a variety of 2-D signal processing operations (104,106,119–136). These processing operations include ambiguity functions, triple correlations, raster format signal spectrum analysis, synthetic aperture radar image formation, and range-Doppler processing. Acousto-optical devices in parallel 2-D optical architectures were employed in these systems because acousto-optical devices have the potential to deliver real-time, wide-bandwidth, processing capabilities required in high-performance radar and communication systems. Early work concentrated on using the Mach–Zehnder interferometer to form coherent high-dynamic-range processors such as the triple-product operation systems. Later, improved mechanical stability incoherent-light in-line architectures were proposed for the triple-product operation. Recently, focus has shifted to coherent in-line processor designs such as using two-beam interference.

Figure 6(a) shows how basically 1-D acousto-optical devices are arranged in space to implement 2-D signal processing transforms. Each acousto-optical device acts as an entry port for a signal waveform that requires processing or is

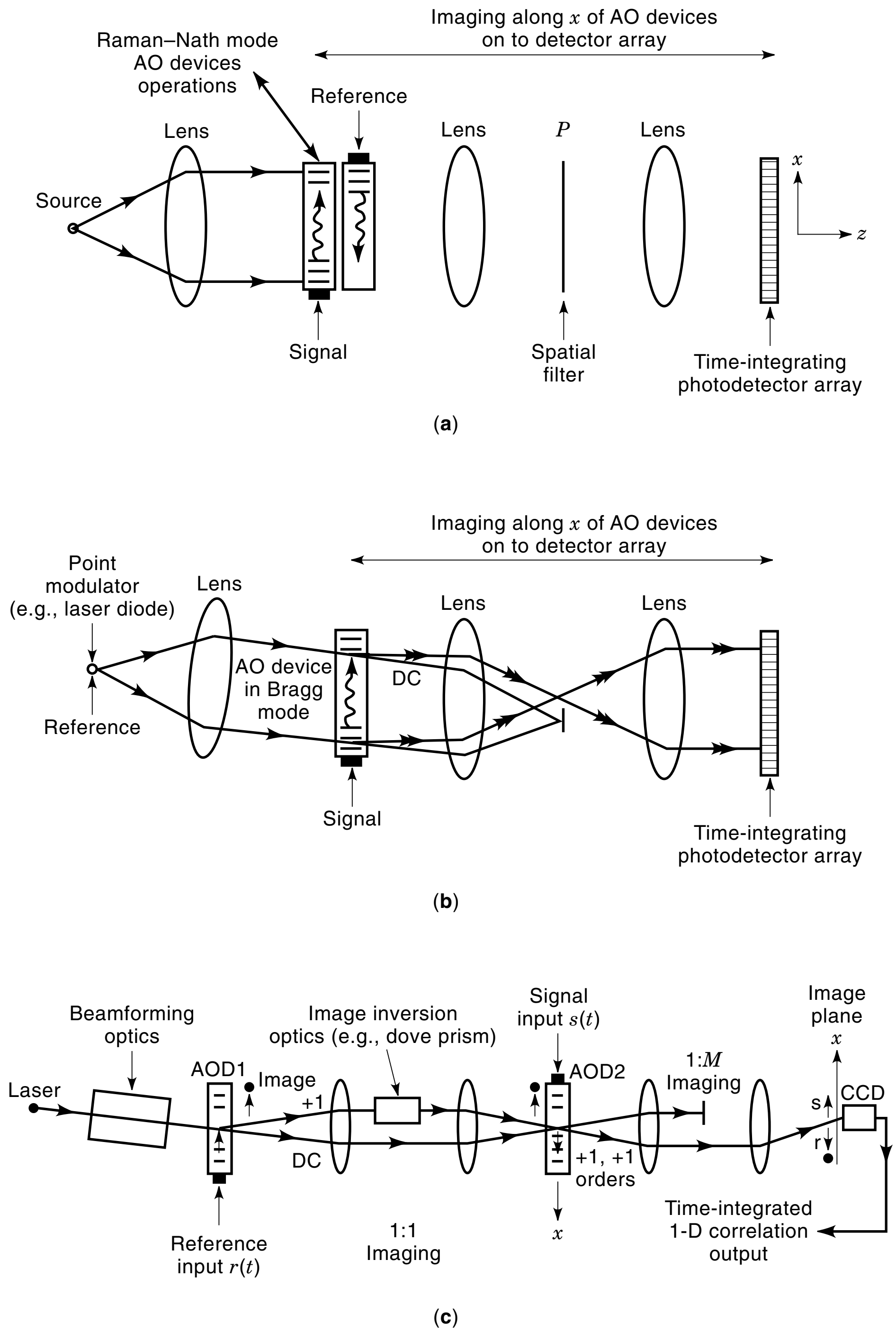

Figure 5. (a) Montgomery two-counter-propagating-acousto-optical-device-based time-integrating correlator design with acousto-optical devices operating in the Raman–Nath mode. To implement the Chirp-Z transform for spectrum analysis, the light source is intensity-modulated by the signal to be analyzed. (b) Sprague and Koliopoulos single-acousto-optical-device-based time-integrating correlator design where both the light source and the Bragg cell are intensity-modulated. (c) Riza coherent interferometric time-integrating correlator design that uses a Dove prism for image inversion and spatial carrier control. Both acousto-optical devices operate in the Bragg mode.

needed to implement a transform using optics. Note that these four acousto-optical devices can also be combined with a modulated light source to provide the system designer other modulation options. Also, the physical orientation of the acousto-optical devices in the x–y coordinate system can be used to generate various output plane coordinates that suit a particular signal processing operation. Typically, acousto-optical cells are positioned orthogonally to generate independent x and y output plane coordinates for two separate signal-processing operations such as one to give a target range location while the other orthogonal coordinate provides the target Doppler information.

One common 2-D signal processing operation in radar is ambiguity function processing. Ambiguity function generation is useful in applications where signals are in a dynamic environment, such as when the received signal can have unknown Doppler shifts and time delays with respect to a transmitted signal. Two key applications for ambiguity function processing are synchronization of pseudorandom sequences in communication receivers and radar target range and velocity

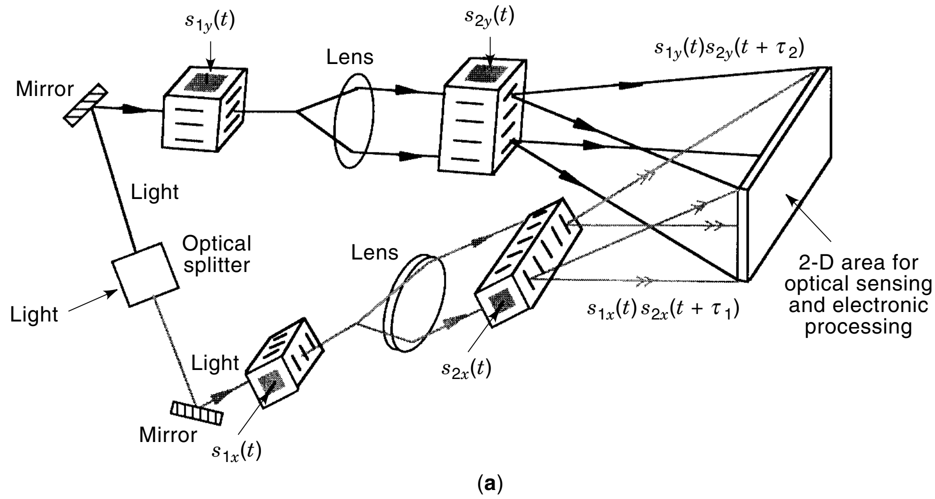

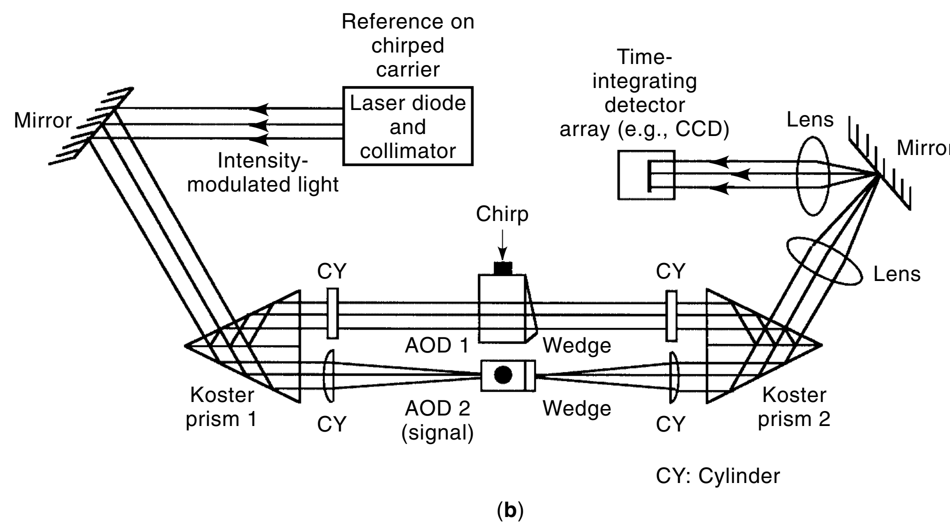

Figure 6. (a) Basic form of the acousto-optical triple-product processor showing how the signals to be processed are fed to the various acousto-optical devices. (b) Two-dimensional acousto-optical range-Doppler processor.

determination. The cross-ambiguity function shown in its symmetric form for signals $r(t)$ and $s(t)$ is defined as

$$A(\tau,\ f_{\mathrm{d}}) = \int_{-\infty}^{+\infty} s(t+\tau/2)r^*(t-\tau/2)\exp(-j2\pi f_{\mathrm{d}}t)\,dt \tag{20}$$

where τ is the time delay and f_{d} is the Doppler shift between the two signals.

One such 2-D acousto-optical ambiguity function processor design proposed for range-Doppler processing is shown in Fig. 6(b) and uses an in-line interferometric design based on Koster prisms, two crossed Bragg cells, and an intensity-modulated laser (128). This time-integrating processor uses a 2-D CCD for time integration. The Chirp-Z transform is used along one output axis for temporal Fourier tranform analysis to produce Doppler information, while the other processor orthogonal axis implements a time-integrating correlation to produce range data or time delay information. The more detailed mathematical treatment of this processor is as follows.

The intensity-modulated light from the laser diode is given by

$$I(t) = I_0\left[1 + m_0\mathrm{Re}\left\{r\left(t-\frac{T}{2}\right)e^{j2\pi(f_1+f_2)(t-T/2)}\,e^{j(\alpha/2)(t-T/2)^2}\right\}\right] \tag{21}$$

where I_0 is the bias term, m_0 is a modulation index, $r(t)$ is the reference waveform, T is the time aperture of the Bragg cells, α is the chirp rate, and f_1 and f_2 are carrier frequencies for Bragg cells AOD1 and AOD2, respectively.

The $+1$ diffracted-order optical field from AOD1 is given by

$$A_1(x,\ t) = \sqrt{\eta_1}e^{j(\alpha/2)(t-T/2-x/v)^2}\,e^{j2\pi f_1(t-T/2-x/v)} \tag{22}$$

where η_1 is the diffraction efficiency for AOD1, and v is the acoustic velocity in AOD1.

Similarly, the -1 diffracted order coming from AOD2 in the spatially orthogonal part of the interferometer is given by

$$A_2(y,\ t) = \sqrt{\eta_2}s^*\left(t-\frac{T}{2}-\frac{y}{v}\right)\,e^{-j2\pi f_2(t-T/2-y/v)} \tag{23}$$

where η_2 is the diffraction efficiency for AOD2, and $s^*(t)$ is the complex conjugate of the input radar return signal.

When we consider unity imaging from the two acousto-optical cells to the CCD plane and taking into account the beam tilt corrections introduced by the two predesigned wedge prisms (seen alongside the Bragg cells), the intensity pattern is given by

$$I(x, y, t) = I(t)|A_1(x, t)e^{j2\pi f_1(x/v)} + A_2(y, t)e^{-j2\pi f_2(y/v)}e^{j2\pi f_s(y/v)}|^2 \quad (24)$$

where f_s/v is an offset spatial carrier introduced in the y direction of the processor output for carrier-based signal demodulation. This intensity pattern is further time-integrated by the CCD for T_c seconds to provide a time integrated charge pattern given by

$$\begin{aligned} Q(x, y) &= \int_0^{T_c} I(x, y, t)\,dt \\ &\sim \text{low spatial frequency bias terms} \\ &\quad + I_0 m_0 \sqrt{\eta_1\eta_2}\,\mathrm{Re}\left\{ e^{-j(\alpha/2)(x/v)^2} e^{j2\pi f_s(y/v)} \int_0^{T_c} \right. \\ &\quad \left. r\left(t-\frac{T}{2}\right) s^*\left(t-\frac{T}{2}-\frac{y}{v}\right) e^{j\alpha(x/v)(t-T/2)}\,dt \right\} \end{aligned} \quad (25)$$

assuming that $T_c \gg 1/(f_1 + f_2)$, which is generally the case with millisecond integration CCDs and radar RF Bragg cell inputs. Recalling the definition of the cross-ambiguity function A_{xy} as

$$A_{xy}(\tau, f_d) = \int_0^{T_c} x(t)y^*(t-\tau)e^{j2\pi f_d t}\,dt \quad (26)$$

we can rewrite $Q(x, y)$ as

$$\begin{aligned} Q(x, y) &= \text{low-frequency biases} \\ &\quad + I_0 m_0 \sqrt{\eta_1\eta_2}\,\mathrm{Re}\left\{ e^{-j(\alpha/2)(x/v)^2} e^{j2\pi f_s(y/v)} A_{rs}\left(\frac{y}{v}, \frac{\alpha x}{2\pi v}\right)\right\} \end{aligned} \quad (27)$$

Hence, neglecting the quadratic phase term in x (it is usually small for typical acousto-optical system design parameters), the charge pattern $Q(x, y)$ is the desired complex range-Doppler image riding on a spectral carrier in the y direction. Hence, the described 2-D acousto-optical processor implements the desired 2-D cross-ambiguity function. A similar analysis approach can be undertaken for other 2-D acousto-optical processors described in the references.

Other Applications of Acousto-optical Devices

Apart from the more traditional applications of acousto-optical devices dealing with analog signal processing mentioned in this article, other applications of acousto-optical devices in analog and digital signal processing continue to appear in the literature. These include the use of the acousto-optical device for transmit–receive phase-based phased array antenna control (137–147), image processing (148–156), binary on/off switching (157–165), continuously variable and switched delay lines (166–171), multiwavelength switched delay lines (172), multiwavelength add–drop cross-connect switches (173), signal excision (174–177), equalization (178), adaptive filtering (179–183), and other applications (187–191).

ACKNOWLEDGMENT

The author would like to acknowledge the assistance provided by graduate student Sarun Sumriddetchkajorn during the preparation of this article.

BIBLIOGRAPHY

1. L. Brillouin, Diffusion de la lumière et des rayons X par un corps transparent homogène, *Ann Phys., Paris,* **17**: 88–122, 1922.
2. C. V. Raman and N. S. N. Nath, The diffraction of light by high frequency sound waves, Part I, *Proc. Indian Acad. Sci.,* **2**: 406–412, 1935.
3. C. V. Raman and N. S. N. Nath, The diffraction of light by high frequency sound waves, Part II, *Proc. Indian Acad. Sci.,* **2**: 413–420, 1935.
4. C. V. Raman and N. S. N. Nath, The diffraction of light by high frequency sound waves, Part III: Doppler effect and coherence phenomenon, *Proc. Indian Acad. Sci.,* **3**: 75–84, 1936.
5. C. V. Raman and N. S. N. Nath, The diffraction of light by high frequency sound waves, Part IV: Generalized theory, *Proc. Indian Acad. Sci.,* **3**: 119–125, 1936.
6. P. Debye and F. W. Sears, On the scattering of light by supersonic waves, *Proc. Natl. Acad. Sci. USA,* **18**: 409–414, 1932.
7. R. Lucas and P. Biquard, Propriétés optiques de smilieux solides et liquides soumis aux vibration élastiques ultra sonores, *J. Phys. Rad.,* **3**: 464–477, 1932.
8. A. P. Goutzoulis and I. J. Abramovitz, Digital electronics meets its match (acoustooptic devices), *IEEE Spectrum,* **25** (8): 21–25, 1988.
9. I. C. Chang, Acoustooptical interactions—a review. I. Acoustooptical devices and applications, *IEEE Trans. Sonics Ultrason.,* **SU-23**: 2, 1976.
10. B. A. Auld, *Acoustic Fields and Waves in Solids,* New York: Wiley, 1973.
11. J. Sapriel, *Acousto-optics,* New York: Wiley, 1979.
12. A. Korpel (ed.), *Selected Papers on Acoustoopticals, SPIE Milestone Series,* Vol. MS 16, SPIE, 1990.
13. C. R. Scott, *Field Theory of Acousto-optic Signal Processing Devices,* Norwood, MA: Artech House, 1992.
14. M. Gottlieb, C. L. M. Ireland, and J. M. Ley, *Electrooptic and Acoustooptic Scanning and Deflection,* Optical Engineering Series, Vol. 3, New York: Marcel Dekker, 1983.
15. J. Xu and R. Stroud, *Acousto-optic Devices: Principles, Design, and Application,* New York: Wiley, 1992.
16. A. P. Goutzoulis and D. R. Pape, *Design and Fabrication of Acousto-optic Devices,* Optical Engineering Series, Vol. 41, New York: Marcel Dekker, 1994.
17. A. Yariv and P. Yeh, *Optical Waves in Crystals,* New York: Wiley, 1984.
18. A. Korpel, Acousto-optics, in R. Wolfe (ed.), *Applied Solid State Science,* Vol. 3, New York: Academic Press, 1972, p. 73.
19. I. C. Chang, Acousto-optic Devices and Applications, in M. Bass (ed.), *Handbook of Optics,* Vol. II, McGraw-Hill, 1995, Chap. 12.
20. I. C. Chang and D. L. Hecht, Characteristics of acousto-optic devices for signal processors, *Opt. Eng.,* **21**: pp. 76–81, 1982.
21. Brimrose Corp. of America, 1998 Product Catalog, Baltimore, MD.
22. NEOS Acousto-optic Products Catalog, Melbourne, FL, 1996.
23. IntraAction Corp. Acousto-optic Products Catalog, Bellwood, IL, 1997.

24. R. G. Rosemeier, J. I. Soos, and J. Rosenbaum, A single element 2-D acousto-optic GaP laser beam steerer, *SPIE Proc.,* **89807**: Los Angeles, 1988.

25. G. S. Kino, *Acoustic Waves-Devices, Imaging, and Analog Signal Processing,* Englewood Cliffs, NJ: Prentice-Hall, 1987.

26. R. G. Hunsperger, *Integrated Optics: Theory and Technology,* Springer Series in Optical Sciences, Vol. 33, 2nd ed., New York: Springer-Verlag, 1985, Chap. 16.

27. P. K. Das and C. M. DeCusatis, *Acousto-optic Signal Processing: Fundamentals and Applications,* Norwood, MA: Artech House, 1991.

28. M. W. Casseday, N. J. Berg, and I. J. Abramovitz, Space Integrating Acousto-optic Signal Processors Using Surface Acoustic Wave (SAW) Delay Lines, in N. J. Berg and J. M. Pellegrino (eds.), *Acousto-optic Signal Processing: Theory and Implementation,* 2nd ed., New York: Marcel Dekker, 1996, pp. 169–206.

29. C. S. Tsai, Optical Modulation: Acousto-Optical Devices, in K. Chang (ed.), *Handbook of Microwave and Optical Components,* Vol. 4; *Fiber and Electro-optical Components,* New York: Wiley, 1991, pp. 199–246.

30. J. Shibata and T. Kajiwara, Optics and electronics are living together, *IEEE Spectrum,* **26** (2): 34–38, 1989.

31. A. Yariv, *Optical Electronics,* 3rd ed., New York: Holt, Rinehart and Winston, 1985, chap. 15.

32. J. Gowar, *Optical Communication Systems, Optoelectronics,* London: Prentice-Hall, 1984.

33. J. W. Goodman, *Introduction to Fourier Optics,* 2nd ed., New York: McGraw-Hill, 1996.

34. F. T. S. Yu and S. Yin, *Selected Papers on Coherent Optical Processing,* SPIE Milestone Series, **MS 52**: SPIE, 1992.

35. J. D. Cohen, Incoherent-Light Time-Integrating Processors, in N. J. Berg and J. M. Pellegrino (eds.), *Acousto-optic Signal Processing: Theory and Implementation,* 2nd ed., New York: Marcel Dekker, 1996, p. 207.

36. J. L. Anderson, H. B. Brown, and B. V. Markevitch, Wideband real-time Fourier analyzer using folded Spectrum techniques, *Proc. SPIE,* **373**: 1981.

37. H. Ansari, B. D. Metscher, and J. R. Lesh, Experimental considerations for 2-D acousto-optic spectrum analysis, *Appl. Opt.,* **29** (36): 5317–5319, 1990.

38. M. Haney and D. Psaltis, Measurement of the temporal coherence properties of pulsed single mode laser diodes, *Appl. Opt.,* **24** (13): 1926, 1985.

39. J. R. Janesick et al., Scientific charge coupled devices, *Opt. Eng.,* **26** (8): 1987.

40. G. M. Borsuk, Photodetectors for acousto-optic signal processors, *Proc. IEEE,* **69**: 100, 1981.

41. G. W. Anderson et al., Role of photodetectors in optical signal processing, *Appl. Opt.,* **27**: 2871, 1988.

42. E. L. Dereniak and G. D. Boreman, *Infrared Detectors and Systems,* New York: Wiley, 1996.

43. U. Efron (ed.), *Spatial Light Modulator Technology: Materials, Devices, and Applications,* New York: Marcel Dekker, 1995.

44. N. A. Riza, Novel acousto-optic systems for spectrum analysis and phased array radar signal processing, Caltech, PhD thesis, 1989.

45. N. A. Riza and D. Psaltis, Optical disk based acousto-optic spectrum analysis, *Annu. Meet. Tech. Digest,* OSA Technical Digest Series, Vol. 15, 1990, p. 73.

46. J. Hong et al., Photorefractive Crystals as Adaptive Elements in Acoustooptic Filters, *Optical Technology for Microwave Applications III, Proc. SPIE,* **789**: SPIE, 1987, pp. 136–144.

47. K. Preston, Use of the Fourier transforming properties of lenses for signal spectrum analysis, in J. T. Tippet et al., (eds.), *Optical and Electrooptical Information Processing,* Cambridge, MA: MIT Press, 1965.

48. D. Casasent, Frequency multiplexed acousto-optic architectures and appliations, *Appl. Opt.,* **24** (6): 856, 1985.

49. A. Vander Lugt, Signal detection by complex spatial filtering, *IEEE Trans. Inf. Theory,* **IT-10**: 139, 1964.

50. D. Casacent (ed.), *Optical Data Processing: Applications,* Topics in Applied Physics, Vol. 23, New York: Springer-Verlag, 1977.

51. S. H. Lee (ed.), *Optical Information Processing: Fundamentals,* New York: Springer-Verlag, 1981.

52. N. J. Berg and J. M. Pellegrino (eds.), *Acousto-optic Signal Processing—Theory and Implementation,* 2nd ed., New York: Marcel Dekker, 1996.

53. P. K. Das, *Optical Signal Processing—Fundamentals,* Berlin: Springer-Verlag, 1991.

54. B. G. Boone, *Signal Processing Using Optics,* New York: Oxford Univ. Press, 1998.

55. A. Vanderlugt, *Optical Signal Processing,* New York: Wiley, 1992.

56. J. L. Horner (ed.), *Optical Signal Processing,* New York: Academic Press, 1987.

57. D. Psaltis and D. Casasent, General formulation for optical signal processing architectures, *Opt. Eng.,* **19** (2): 193–198, 1980.

58. W. T. Rhodes, Acousto-optic algebraic processing architectures, *Proc. IEEE* **72**: 820–830, 1984.

59. Y. S. Abu-Mostafa and D. Psaltis, Optical neural computers, *Sci. Amer.,* **256** (3): 66–73, 1987.

60. D. Psaltis and N. Farhat, Optical information processing based on an associative memory model of neural nets with thresholding and feedback, *Opt. Lett.,* **10** (2): 1985.

61. D. Psaltis, E. G. Paek, and J. Hong, Acousto-optic implementation of the Hopfield model, *J. Opt. Soc. Amer.,* **2** (13): 48, 1985.

62. N. H. Farhat et al., Optical Implementation of the Hopfield Model, *Appl. Opt.,* **24**: 1469, 1985.

63. P. Kellman, Time integrating optical signal processing, *Opt. Eng.,* **19** (3): 370, 1980.

64. K. Wagner, Time and space integrating acousto-optic signal processing, PhD thesis, chap. 4, Caltech, 1987.

65. R. P. Bocker, K. Bromley, and S. R. Clayton, A Digital Optical Architecture for Performing Matrix Algebra, in K. Bromley (ed.), *Real-Time Signal Processing VI, Proc. SPIE,* **431**: SPIE, 1983, p. 194.

66. R. A. Sprague and C. L. Koliopoulos, Time integrating acousto-optic correlator, *Appl. Opt.,* **15** (1): 89, 1976.

67. H. Ansari and J. R. Lesh, Superfine resolution acousto-optic spectrum analysis, *Appl. Opt.,* **30** (11): 1396, 1991.

68. D. F. Barbe, Imaging devices using the charge coupled concept, *Proc. IEEE,* **63**: 38–67, 1975.

69. D. Psaltis, Optical image correlation using acouto-optic and charge-coupled devices, *Appl. Opt.,* **21**: 491–495, 1982.

70. N. A. Riza and D. Psaltis, Acousto-optic signal processors for transmission and reception of phase array antenna signals, *Appl. Opt.,* **30** (23): 3294, 1991.

71. M. W. Haney, Compact acousto-optic processor for synthetic aperture radar image formation, *Proc. IEEE,* **82**: 1735–1748, 1994.

72. D. Psaltis, J. Yu, and J. Hong, Bias-free time integrating optical correlator using a photorefractive crystal, *Appl. Opt.,* **24** (22): 3860–3865, 1985.

73. D. Psaltis, Two dimensional optical processing using one dimensional input devices, *Proc. IEEE,* **72**: 962–972, 1984.

74. D. Psaltis and D. Casasent, Time and space integrating spectrum analyzer, *Appl. Opt.,* **18**: 3203, 1979.

75. T. R. Bader, Acoustooptic spectrum analysis: A high performance hybrid technique, *Appl. Opt.,* **18** (10): 1979.

76. K. Wagner and D. Psaltis, Time and space integrating acousto-optic folded spectrum processing for SETI, *Proc. SPIE,* **564-31**: 1985.

77. H. Ansari, B. D. Metscher, and J. R. Lesh, Experimental considerations for 2-D acousto-optic spectrum analysis, *Appl. Opt.,* **29** (36): 5317, 1990.

78. D. Casasent, General time, space and frequency multiplexed acousto-optic correlator, *Appl. Opt.,* **24** (17): 1985.

79. L. B. Lambert, Wideband instantaneous spectrum analyzers employing delay line light modulators, *IRE Natl. Conv. Rec.,* **10** (6): 9, 1962.

80. I. C. Chang, Acousto-optic channelized receiver, *Microw. J.,* **29** (3): 141–157, 1986.

81. M. C. King et al., Real-time electro-optical signal processors with coherent detection, *Appl. Opt.,* **6**: 1367, 1967.

82. A. Vaner Lugt, Interferometric spectrum analyzer, *Appl. Opt.,* **20** (16): 2770–2779, 1981.

83. M. L. Shah et al., Interferometric Bragg cell spectrum analyzer, *IEEE Ultrasonic Symp. Proc.,* **2**: 743–746, 1981.

84. I. C. Chang, R. Lu, and L. S. Lee, High Dynamic Range Acousto-optic Receiver, in *Optical Technology for Microwave Applications II,* Proc. Soc. Photo-Opt. Instrum. Eng. **545**, 1985, pp. 95–101.

85. J. B. Tsui, I. C. Chang, and E. Gill, Interferometric Acousto-optic Receiver, in *Optical Technology for Microwave Applications IV,* Proc. Soc. Photo-Opt. Instrum. Eng. **1102**, 1989, pp. 176–182.

86. M. D. Koontz, Miniature Interferometric Spectrum Analyzer, in *Optical Information Processing II,* Proc. Soc. Photo-Opt. Instrum. Eng. **639**, 1986, pp. 126–130.

87. N. A. Riza, Optically efficient interferometric acousto-optic architecture for spectrum analysis, *Appl. Opt.,* **31** (17): 3194–3196, 1992.

88. G. D. Xu and C. S. Tsai, Integrated acousto-optic modules for interferometric RF spectrum, *IEEE Photonics Technol. Lett.,* **3**: 153–155, 1991.

89. L. Jakab and P. Richter, Interferometric scanning acousto-optic spectrum analysis, *Appl. Opt.,* **30** (10): 1206–1209, 1991.

90. G. J. Farley and P. Galko, Acousto-optic spectrum analyzer techniques for monitoring CW, *IEEE Trans. Aerosp. Electron. Syst.,* **27**: 430–440, 1991.

91. S. Zohar, Spectral window of the acousto-optic folded spectrum analyzer, *Appl. Opt.,* **32** (32): 6445–6455, 1993.

92. T. Turpin, Time integrating optical processing, *Proc. SPIE,* **154**: 196, 1978.

93. C. E. Thomas, Optical spectrum analysis of large space bandwidth signals, *Appl. Opt.,* **5**: 1782, 1986.

94. G. Lebreton, Power spectrum of rastered scanned signals, *Opt. Acta,* **29** (4): 413, 1982.

95. W. T. Rhodes, The falling raster in optical signal processing, *Proc. SPIE,* **373**: 1981.

96. T. R. Bader, Coherent hybrid optical processors, *Proc. SPIE,* **232**: 1980.

97. S. K. Kniffen, M. F. Becker, and E. J. Powers, Bispectral magnitude and phase recovery using a wide bandwidth acousto-optic processor, *Appl. Opt.,* **31** (8): 1015–1029, 1992.

98. A. H. Rosenthal, Application of ultrasonic light modulation to signal recording, display, analysis and communication, *IRE Trans. Ultrason. Eng.,* **SU-8**: 1, 1961.

99. L. Slobodin, Optical correlation technique, *Proc. IEEE,* **512**: 1782, 1963.

100. E. B. Felstead, A simplified coherent optical correlator, *Appl. Opt.,* **7** (1): 105–108, 1968.

101. R. M. Montgomery, Acousto-optic signal processing system, US patent 3,634,749, Jan., 1972.

102. R. A. Sprague and C. L. Koliopoulos, Time integrating acoustooptic correlator, *Appl. Opt.,* **15** (1): 89, 1976.

103. R. A. Sprague, A review of acousto-optic signal correlators, *Opt. Eng.,* **16** (5): 467–474, 1977.

104. W. T. Rhodes, Acousto-optic signal processing: convolution and correlation, *Proc. IEEE,* **69**: 65–78, 1981.

105. N. J. Berg et al., Surface wave delay line acoustooptic devices for signal processing, *Appl. Opt.,* **18** (16): 2767–2774, 1985.

106. T. M. Turpin, Spectrum analysis using optical processing, *Proc. IEEE,* **69**: 79–92, 1981.

107. R. D. Griffin and J. N. Lee, Acousto-optic wideband correlator system: Design, implementation, and evaluation, *Appl. Opt.,* **33** (29): 6774–6787, 1994.

108. L. R. Rabiner et al., The Chirp-Z algorithm, *IEEE Trans. Audio Electroacoust.,* **AU-17**: 86, 1969.

109. J. N. Lee and A. VanderLugt, Acousto-optic signal processing and computing, *Proc. IEEE,* **77**: 1528–1557, 1989.

110. N. A. Riza, In-line interferometric time integrating acoustooptic correlator, *Appl. Opt.,* **33** (14): 3060–3069, 1994.

111. H. G. Andrews II, M. E. Turbyfill, and C. W. Keefer, Anti-jamming Optical Beam-Forming Systems, in A. R. Pirich and P. Sierak (eds.), *Photonics at the Air Force Photonics Center, Proc. SPIE,* **2216**, SPIE, 1994, pp. 58–66.

112. C. W. Keefer, M. E. Turbyfill, and H. G. Andrews II, Multichannel Acousto-optic Correlator for Time-Delay Computation, in D. R. Pape (ed.), *Advances in Optical Information Processing VI, Proc. SPIE,* **2240**, SPIE, 1994, pp. 64–74.

113. J. M. Lutsko et al., Multichannel In-Line Interferometric Time-Integrating Correlator and Its Applications, in A. R. Pirich (ed.), *Photonic Device Engineering for Dual-Use Applications, Proc. SPIE,* **2481**, SPIE, 1995, pp. 153–159.

114. P. A. Wasilousky et al., Optoelectronic radar receiver for real-time radar imaging, in W. J. Miceli (ed.), *Radar/Ladar Processing and Applications, Proc. SPIE,* **2562**, SPIE, 1995, pp. 44–55.

115. P. A. Wasilousky, T. A. Sunderlin, and T. Olmstead, Characterization of Wideband ISAR Processor, in D. R. Pape (ed.), *Advances in Optical Information Processing VII, Proc. SPIE,* **2754**, SPIE, 1996, pp. 31–39.

116. T. Omstead, T. A. Sunderlin, and P. A. Wasilousky, Preliminary Characterization of a Hybrid Optical-Digital ISAR Processor, in W. J. Miceli (ed.), *Radar Processing, Technology, and Applications, Proc. SPIE,* **2845**, SPIE, 1996, pp. 211–220.

117. N. A. Riza, Novel Space/Time Integrating Acoustooptic Architectures for Radar Signal Processing, in *Optoelectronic Signal Processing for Phase Array Antennas IV Conference Proceedings of the SPIE,* **2155**, SPIE, 1994, pp. 413–419.

118. N. A. Riza, Space integrating interferometric acousto-optic convolver, *IEEE Photonics Technol. Lett.,* **7**: 339–341, 1995.

119. R. A. K. Said and D. C. Cooper, Crosspath real-time optical correlator and ambiguity function processor, *Proc. IEE,* **120**: 423, 1973.

120. P. Kellman, Time integrating optical processors, *SPIE Proc.,* **154**: 196, 1978.

121. P. Kellman, Time integrating optical signal processing, PhD thesis, Stanford University, Stanford, CA, 1979.

122. I. J. Abramovitz, N. J. Berg, and M. W. Casseday, Interferometric surface wave acousto-optic time integrating correlators, *Proc. IEEE Ultrasonic Symp.,* Boston, 1980, pp. 483–486.

123. J. D. Cohen, Ambiguity processor architectures using one di-

mensional acousto-optic transducers, *Proc. SPIE,* **180**: 134, 1979.

124. A. W. Lohmann and B. Wirnitzer, Triple correlations, *Proc. IEEE,* **72**: 889, 1984.
125. A. VanderLugt, Crossed Bragg cell processors, *Appl. Opt.,* **23**: 2275, 1984.
126. M. A. Krainak and D. E. Brown, Interferometric triple product processor (almost common path), *Appl. Opt.,* **24**: 1385, 1985.
127. J. D. Cohen, High bandwidth triple product processor using a shearing interferometer, *Appl. Opt.,* **24** (19): 3173–3178, 1985.
128. L. Harrison et al., Acousto-optic range Doppler processor for radar insertion, *SPIE Proc.,* **1958**: 71–82, 1993.
129. K. R. Frampton et al., Acouto-optic range Doppler processor performance, *SPIE Proc.,* **256207**: 1995.
130. D. C. Hartup and W. T. Rhoes, Acousto-optic processor for carrier frequency and envelope modulation analysis, *SPIE Proc.,* **1704**: 98–104, 1992.
131. B. Tasic and V. M. Ristic, Triple product optical processor for analysis of pulse-repetition and carrier frequencies of radar signals, *Appl. Opt.,* **34** (35): 8144–8147, 1995.
132. D. Psaltis and K. Wagner, Real-time optical synthetic aperture radar (SAR) processor, *Opt. Eng.,* **21** (5): 1982.
133. M. Haney and D. Psaltis, Real-time programmable acoustooptic synthetic aperture radar processor, *Appl. Opt.,* **27** (9): 1998.
134. C. C. Aleksoff, N. S. Subotic, and I. Cindrich, Time Integrating compact hybrid optical processor for SAR image formation, *Proc. SPIE,* **1704**: 43–58, 1992.
135. N. A. Riza, Multi-function Acousto-optic Signal Processor, in D. R. Pape (ed.), *Advances in Optical Information Processing VIII, Proc. SPIE,* **3388**, No. 9, SPIE, 1998.
136. N. A. Riza and D. R. Pape, Photonic Signal Processing for Inverse Synthetic Aperture Radar Imaging, in D. R Pape (ed.), *Advances in Optical Information Processing VIII, Proc. SPIE,* **3388**, No. 9, SPIE, 1998.
137. M. Tamburrini et al., Optical feed for a phased array microwave antenna, *Electron. Lett. 1987,* **23** (13): 680–681, 1987.
138. I. C. Chang and S. S. Tarng, Phased Array Beamforming Using Acousto-optic Techniques, in D. R. Pape (ed.), *Advances in Optical Information Processing III, Proc. SPIE,* **936**, SPIE, 1988, pp. 163–167.
139. N. A. Riza and D. Psaltis, Acousto-optic signal processors for transmission and reception of phased-array antenna signals, *Appl. Opt. 1991,* **30** (23): 3294–3303, 1991.
140. N. A. Riza, An acousto-optic phased array antenna beamformer for multiple simultaneous beam generation, *IEEE Photonics Technol. Lett.,* **4**: 807–809, 1992.
141. N. A. Riza, An acousto-optic phased array antenna beamformer with independent phase and carrier control using single sideband signals, *IEEE Photonics Technol. Lett.,* **4**: 177–179, 1992.
142. N. A. Riza, A compact high-performance optical control system for phased array radars, *IEEE Photonics Technol. Lett.,* **4**: 1072–1075, 1992.
143. N. A. Riza, Liquid crystal-based optical control of phased array antennas, *J. Lightwave Technol.,* **10** (12): 1974–1984, 1992.
144. N. A. Riza, Acousto-optic liquid-crystal analog beam former for phased-array antennas, *Appl. Opt. 1994,* **33** (17): 3712–3724, 1994.
145. N. A. Riza, Acousto-optic architecture for two dimensional beam scanning in phased array antennas, *Appl. Opt.,* **31** (17): 3278–3284, 1992.
146. N. A. Riza, Experimental demonstration of an acoustooptic system for two dimensional phased array antenna scanning, *Appl. Opt.,* **32** (11): 1936–1942, 1993.
147. N. A. Riza, Photonic processor for in-phase and quadrature array signal processing, *SPIE Proc.,* **2754**, 50–64, 1996.
148. P. A. Molley and K. T. Stalker, Acousto-optic signal processing for real-time image recognition, *Opt. Eng.,* **29**: 1073–1080, 1990.
149. T. C. Poon and A. Korpel, Optical transfer function of an acousto-optic heterodyning image processor, *Opt. Lett.,* **4**: 317–319, 1992.
150. J. N. Mait, D. W. Prather, and R. A. Athale, Crossed Bragg cell implementation of a Fourier-plane filter for optical image correlator, *Appl. Opt.,* **31**: 6820–6822, 1992.
151. T. P. Karnowski and A. Vanderlugt, Generalized filtering in acousto-optic system using area modulation, *Appl. Opt.,* **30** (17): 2344–2353, 1991.
152. N. Goto, Y. Kanayama, and Y. Miyazaki, Integrated optic matrix–vector multiplier using multifrequency acousto-optic Bragg diffraction, *Appl. Opt.,* **30** (5): 523–530, 1991.
153. R. A. Athale, J. N. Mait, and D. W. Prather, Optical morphological image processing with acoustooptic devices, *Opt. Commun.,* **87**: 99–104, 1992.
154. J. N. Mait, D. W. Prather, and R. A. Athale, Acoustooptic processing with electronic feedback for morphological filtering, *Appl. Opt.,* **31**: 5688–5699, 1992.
155. D. Psaltis, Incoherent electro-optic image correlator, *Opt. Eng.,* **23** (1): 12–15, 1984.
156. E. G. Paek et al., Nonmechanical image rotation with an acousto-optic dove prism, *Opt. Lett.,* **22** (15): 1195–1197, 1997.
157. W. E. Stephens et al., Demonstration of a photonic space switch utilizing acousto-optic elements, *Opt. Eng.,* **29** (3): 183–190, 1990.
158. D. O. Harris and A. Vanderlugt, Acousto-optic photonic switch, *Opt. Lett.,* **14** (21): 1177–1179, 1989.
159. D. O. Harris, Multichannel acousto-optic crossbar switch, *Appl. Opt.,* **30**: 4245–4256, 1991.
160. D. O. Harris and A. Vanderlugt, Multichannel acousto-optic crossbar switch with arbitrary signal fan-out, *Appl. Opt.,* **32**: 1684–1686, 1992.
161. M. L. Wilson, D. L. Fleming, and F. R. Dropps, A fiber optic matrix switchboard using acoustooptic Bragg cells, *SPIE* , **988**: 56–62, 1988.
162. K. Wagner et al., Low-Loss Acousto-optic Permutation Interconnection Networks, in H. S. Hinton and J. W. Goodman (eds.), *OSA Proceedings on Photonic Switching,* Salt Lake City, UT, **8**, 1991.
163. K.-Y. Wu et al., A novel acoustooptic photonic switch, *Proc. SPIE,* **1563**: 1991.
164. R. Mcleod et al., Acoustooptic Crossbar Photonic Switch, in J. W. Goodman (ed.), *OSA Proceedings on Photonic Switching,* 1993.
165. N. A. Riza, Acousto-optic device-based high speed high isolation photonic switching fabric for signal processing, *Opt. Lett.,* **22** (13): 1003–1005, 1997.
166. S. H. Lin and R. S. Boughton, Acousto-optic Multichannel Programmable True Time Delay Lines, in S.-K. Yao (ed.), *Optical Technology for Microwave Applications IV, Proc. SPIE,* **1102**, SPIE, 1989, pp. 162–173.
167. E. N. Toughlian and H. Zmuda, A photonic variable RF delay line for phased array antennas, *J. Lightwave Technol. 1990,* **8** (12): 1824–1828, 1990.
168. E. H. Monsay, K. C. Baldwin, and M. J. Caccuitto, Photonic true time delay for high-frequency phased array systems, *IEEE Photonics Technol. Lett.,* **6**: 118–120, 1994.
169. W. D. Jemison and P. R. Herczfeld, Acoustooptically controlled true time delays, *IEEE Microw. Guided Wave Lett.,* **3**: 72–74, 1993.
170. L. H. Gesell et al., Acousto-optic Control of Time Delays for

Array Beam Steering, in B. M. Hendrickson (ed.), *Optoelectronic Signal Processing for Phased-Array Antennas IV, Proc. SPIE,* **2155**, 1994, pp. 194–204.

171. N. A. Riza, Acoustooptically switched optical delay lines, *Opt. Commun.,* **145**: 15–20, 1998.
172. N. A. Riza, Photonically controlled ultrasonic arrays: Scenarios and systems, *IEEE Int. Ultrason. Symp. Dig.,* 1996, pp. 1545–1550.
173. N. A. Riza and Jian Chen, Ultra-high −47 dB optical drop rejection multi-wavelength add–drop filter using spatial filtering and dual bulk acousto-optic tunable filters, *Opt. Lett.,* **23** (12): 945–947, 1998.
174. J. Erickson, Optical excisor performance limits versus improved signal detection, *Proc. SPIE,* **639**: 232, 1986.
175. E. R. Raudenbush, Acousto-optic interferometric signal excisor, *Proc. SPIE,* **936**: 168–173, 1988.
176. R. W. Brandstetter and P. G. Grieve, Excision of interference from radio frequency signals by means of a recursive optical notching filter, *Opt. Eng.,* **29** (7): 804–815, 1990.
177. R. N. Ward and A. Vanderlugt, Signal distortion in an adaptive excision system, *Opt. Eng.,* **31** (3): 606–613, 1992.
178. C. S. Anderson, Acousto-optic channel equilization for microwave digital radios, *Appl. Opt.,* **32** (23): 4388–4397, 1993.
179. D. Casasent, Optical processing for adaptive phased-array radar, *IEE Proc.,* **127F** (4): 278, 1980.
180. D. Psaltis and J. Hong, Adaptive acoustooptic filter, *Appl. Opt.,* **23** (19): 3475–3481, 1984.
181. R. M. Montgomery and M. R. Lange, Photorefractive adaptive filter structure with 40dB interference rejection, *Appl. Opt.,* **30** (20): 2844–2849, 1991.
182. R. M. Iodice and P. H. Ruterbusch, Acousto-optic Null Steering Processor (AONSP) Hardware Performance Summary, in D. P. Casasent (ed.), *Transition of Optical Processors into Systems 1995, Proc. SPIE,* **2489**, SPIE, 1995, pp. 45–64.
183. R. T. Weverka, K. Wagner, and A. Sarto, Photorefractive processing for large adaptive phased-arrays, *Appl. Opt.,* **35**: 1344–1366, 1996.
184. C. Garvin and K. Wagner, Real-time signal classification with an acousto-optic triple-product processor cascaded into a volume holographic classifier, *Appl. Opt.,* **35** (20): 3937–3944, 1996.
185. J. H. Hong and T. Y. Chang, Adaptive Signal Processing with Photorefractive Systems, in D. P. Casasent (ed.), *Transition of Optical Processors into Systems 1995, Proc. SPIE,* **2489**, SPIE, 1995, pp. 36–44.
186. N. A. Riza, Acousto-optic null steering adaptive photonic processor architecture for phased arrays, *SPIE Proc.,* **2754**: 95–102, 1996.
187. C. DeCusatis, P. Das, and D. M. Litynski, Acousto-electro-optic phase gratings for optical signal processing applications, *Appl. Opt.,* **30** (5): 583–596, 1991.
188. J. B. G. Roberts, Role for optical signal and image processing in the VLSI era, *IEE Proc.,* **133** (1): 2–6, 1986.
189. E. Tervonen et al., Programmable otical interconnections by multilevel synthetic acousto-optic holograms, *Opt. Lett.,* **16**: 1274–1276, 1991.
190. D. Psaltis, M. A. Neifeld, and A. A. Yamamura, Optical memory disks in optical information processing, *Appl. Opt.,* **29** (14): 2038, 1990.
191. L. N. Flores and D. L. Hecht, Acousto-optic signal processors, *Proc. SPIE,* **128**: 118, 1977.

NABEEL A. RIZA
University of Central Florida